environmental microbiology

Environmental Microbiology (2016) **18**(11), 3932–3948 doi:10.1111/1462-2920.13391

Linking internal and external bacterial community control gives mechanistic framework for pelagic virus-to-bacteria ratios

Selina Våge,* Bernadette Pree and T. Frede Thingstad

Department of Biology, University of Bergen and Hjort Centre for Marine Ecosystem Dynamics, N-5020 Bergen, Norway.

Summary

For more than 25 years, virus-to-bacteria ratios (VBR) have been measured and interpreted as indicators of the importance of viruses in aquatic ecosystems, yet a generally accepted theory for understanding mechanisms controlling VBR is still lacking. Assuming that the denominator (total bacterial abundance) is primarily predator controlled, while viral lysis compensates for host growth rates exceeding this grazing loss, the numerator (viral abundance) reflects activity differences between prokaryotic hosts. VBR is then a ratio between mechanisms generating structure within the bacterial community and interactions between different plankton functional types controlling bacterial community size. We here show how these arguments can be formalized by combining a recently published model for co-evolutionary host-virus interactions, with a previously published "minimum" model for the microbial food web. The result is a framework where viral lysis links bacterial diversity to microbial food web structure and function, creating relationships between different levels of organization that are strongly modified by organism-level properties such as cost of resistance.

Introduction

Rooted in substantial theoretical and experimental evidence, there is a general acknowledgement of viruses exerting a significant top-down control on the biodiversity inside the heterotrophic prokaryote community [henceforth termed bacterial community] (Thingstad, 2000; Brussaard, 2004; Weinbauer, 2004; Suttle, 2007; Winter *et al*., 2010), presumably in interaction with bottom-up mechanisms related to substrate diversity and generalist versus specialist strategies (e.g., Mou *et al*., 2008) in the hosts' use of complex substrates available in most natural environments. Viral lysis also diverts the transfer of energy and material up the predatory food chain towards higher trophic levels; shunting it instead back to detritus and dissolved material (Fuhrman, 1999; Wilhelm and Suttle, 1999; Weinbauer, 2004; Suttle, 2007) with reduced food chain transfer efficiency as an important ecosystem consequence. Viral lysis is therefore an obvious candidate for a mechanism generating biodiversity-ecosystem function (BEF) relationships in the microbial part of the pelagic food web.

As a measure of viral influence in aquatic environments, virus-to-bacteria ratios (VBR) have been reported for more than 25 years (Ogunseitan *et al*., 1990; Wommack and Colwell, 2000; Wigington *et al*., 2016). While viruses are typically considered to be tenfold more abundant than their microbial hosts, data actually show that ratios vary substantially on regional and global scales (Wigington *et al*., 2016). However, a generally accepted theoretical framework within which these values could be understood and analyzed has been missing. Partly this may be rooted in a segregation of directions within aquatic microbial ecology: Following the introduction of the concept of a "microbial loop" (Azam *et al*., 1983), many studies fruitfully treated the community of heterotrophic bacteria as one plankton functional type (PFT), without resolving its internal structure. In contrast, the development from around 1990 of molecular techniques powerful enough to analyze samples from complex systems (Giovannoni *et al*., 1990; Øvreås *et al*., 1997) led to a new focus, where resolving internal structure and diversity of aquatic bacterial communities became a primary research goal. The next step of linking internal structure and function of the bacterial community to the outer level of microbial food web dynamics remains, however, a major challenge in aquatic microbial ecology.

The obvious need for tools that can serve as a theoretical analysis of these relationships led us to explore the consequences of combining two published models: (1)

Received June, 2015; accepted May, 2016. *For correspondence. E-mail: selina.vage@uib.no; Tel. (+0047) 942 135 81.

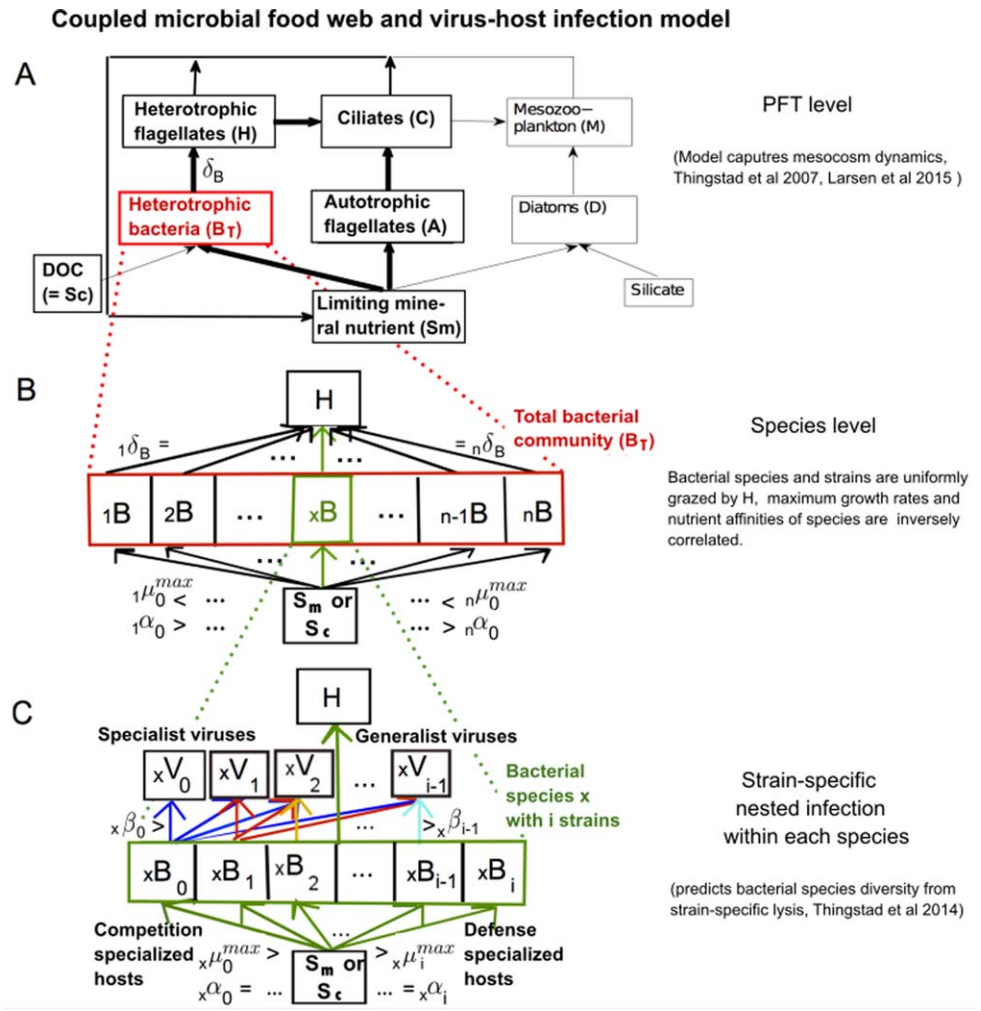

Fig. 1. Schematic of merged model components with different resolutions.
A: "Minimum" microbial food web model (Thingstad *et al*., 2007) resolving interactions between PFTs. Top-down cascading effects from ciliate grazing control total bacterial abundance, while bacterial growth is indirectly controlled by ciliates through the link of autotrophic flagellates and limiting mineral nutrient. B, C: Virus-host interaction model with nested infection resolving bacterial species and strains. Nested infection is conceived through virus-host co-evolution towards more resistance in hosts and broader host range in viruses (Martiny *et al*., 2014). Bacterial species *x* is shown with *i* strains for illustrative purpose. The first strain of species *x* acquiring resistance to the original virus, ${}_xB_1$, evolves from the susceptible parent strain ${}_xB_0$ at the cost of reduced maximum growth rate ${\mu_0}^{max}$, and mutants of the original virus ${}_xV_0$ gain an increasing host range to reinfect resistant strains at the cost of reduced adsorption coefficients β (Supporting Information 5). Host strains of species *x* with low indices (left in Fig. 1C) established early during arms-race dynamics and are specialized in competition for the limiting resource (S_m or S_c), whereas host strains with high indices (right in Fig. 1C) evolved later during this arms-race after undergoing several resistance mutations. These later evolved strains are thus defense specialists with reduced maximum growth rates (${\mu_0}^{max} < {\mu_i}^{max}$). Viruses with low indices (top left in Fig. 1C) are viruses present since early on in the arms-race and are specialized to infect ancient host strains only, whereas the later evolved viruses (top right in Fig. 1C) have accumulated expanding host range mutations and are thus generalists able to infect both ancient and recently evolved host strains, but with reduced effective adsorption coefficients (${\beta_0}^{max} < {\beta_{i-1}}^{max}$). For details, see text.

The "minimum" food web model used, for example, by Larsen *et al*. (2015) to synthesize results from mesocosms with seemingly different responses (Fig. 1A) and (2) the host-virus interaction model based on conceived arms-race dynamics discussed by Thingstad *et al*. (2014) resolving both "species" and "strains" in the community (Fig. 1B and C). This gives, to the best of our knowledge, the first study that combines virus-host interactions and resulting species and strain diversity within the bacterial community, with mechanisms controlling food web structure on the level of PFTs.

The dynamic perspectives of such a combined model are intriguing since it implies the blending of evolutionary and ecological processes occurring on overlapping time scales (days-weeks). Here, however, we analyze only the steady state solutions of this combined model, assuming both that the evolutionary arms races between hosts and viruses have reached maturation (Thingstad *et al*., 2014)

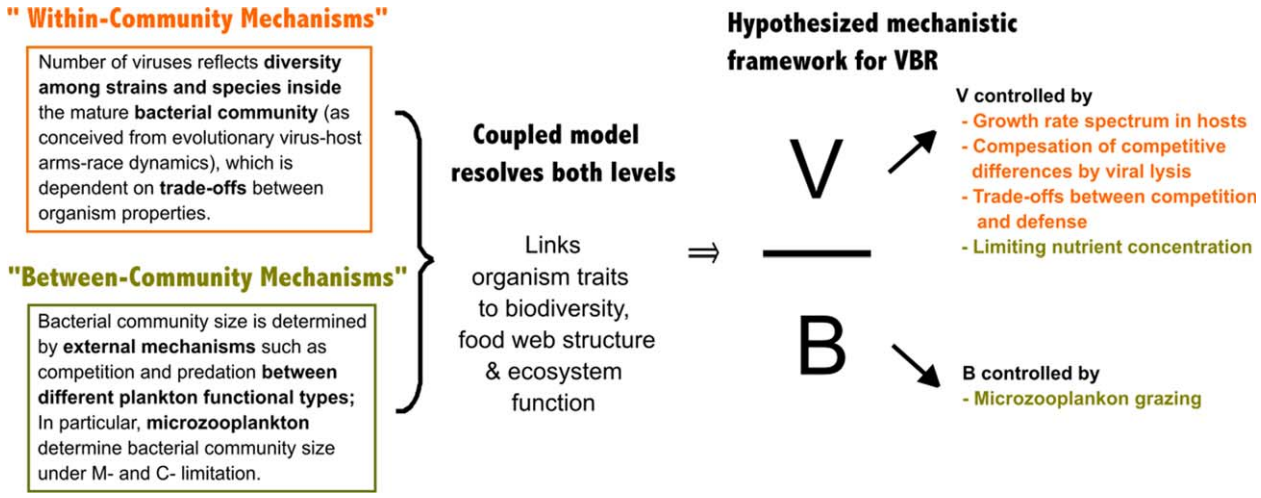

Fig. 2. Conceptual figure of coupled model that combines "within-community control" with "between-community control." VBR emerges in this model as the ratio of a combination of internal and external control mechanisms. Total virus abundance is controlled by external factors such as limiting resource concentration (which under M-limitation is controlled by ciliate abundance) and internal factors such as COR against viral lysis, which gives a range of competitive abilities in the host population, where competitively superior strains support higher viral abundances at steady state. The efficiency by which BP is transferred to higher trophic levels and/or exported to the deep ocean depends on the amount of viruses and thus a combination of these factors. Total bacterial abundance is in our model controlled more uniformly by microzooplankton grazing (see text).

and that the ecological processes of growth and loss are in balance.

The result is a hypothesis for how VBR may be linked to cost of viral defense, biodiversity and ecosystem function. In particular, the framework allows us to analyze how trade-offs between competitive and defensive abilities of host strains and diversity inside the bacterial community may be linked to viral abundance, while mechanisms acting between different PFTs may regulate total bacterial community size (Fig. 2).

In the following, we summarize the theory and describe the methods to derive the discussed relationships. The biologically relevant details of the model are presented and discussed in the Results and Discussion section. For ease of reading, most of the technical mathematical derivations of the relationships and the Matlab code used for the calculations are moved to the Supporting Information (Model Equations and Code 1 and 2).

Theory and methods

Combined model

We obtained the desired framework by combining two previously published models that use different levels of trophic resolution: One "minimum" food web model (Fig. 1A) that resolves PFTs to the community level (Thingstad *et al.*, 2007), including a bacterial community); and one host-virus interaction model (Fig. 1B and C) that resolves the bacterial community to the species and strains (Thingstad *et al.*, 2014).

Briefly, the "minimum" PFT model represents a phosphorous cycle driven by the trophic interactions between six PFTs: bacteria, autotrophic and heterotrophic flagellates, ciliates, diatoms and mesozooplankton (Fig. 1A). This creates three pathways for mineral nutrients into the food web: through bacteria, autotrophic flagellates and diatoms, respectively. The actual flow in a given situation depends on the competitive and predatory trophic interactions between the six PFTs, modified by a possible limitation by lack of degradable organic substrates (such as DOC) for bacterial growth and/or a lack of silicate required for diatom growth. For bacteria, this model thus allows for two states: mineral nutrient limited (M-limited) or limited by organic substrates (C-limited).

The PFT food web model has the power to explain seemingly conflicting results from mesocosm experiments, such as different response patterns of PFTs following identical treatments, depending on the initial state of the system (Larsen *et al.*, 2015). Comparing population dynamics in mesocosm experiments in different environments, Larsen *et al.* (2015) found that ciliate abundance plays a key role in the food-web control of bacterial abundance and growth. Briefly, ciliate grazing on flagellates creates two trophic cascades (Fig. 1A): one via heterotrophic flagellates to bacterial abundance (top-down control of bacteria) and one via autotrophic flagellates to the concentration of growth rate limiting mineral nutrients (assumed to be phosphate in this model, bottom-up control of bacteria). In the case of mineral nutrient-limited bacterial growth, ciliate abundance thus controls both bacterial abundance and bacterial growth rate. Based on the

observed connection between ciliate abundance and bacteria-virus community structures, we use ciliate abundance as the independent variable that sets the carrying capacity of the bacterial community, that is, we calculate how the combined model's steady state solutions depend on ciliate abundance.

Assuming food uptake to be proportional to food concentration linearizes the steady state equations and allows analytical solutions that relate the steady state values for the PFTs (Thingstad *et al*., 2007). Hence, this linearization is used in the subsequent analysis. We note that the linear approximation can be justified biologically in the oligotrophic pelagic, where uptake rates are limited by external resources rather than internal handling time.

For ease of reference, the equations describing steady state for the microbial communities in the PFT food web model used here and properties of this steady state are reproduced from Thingstad *et al*. (2007) in the Supporting Information 1. For completeness, the dynamic equations from which the steady-states are derived are given in Supporting Information 8.

The host-virus interaction model (Fig. 1B) was analyzed in detail for an idealized chemostat environment in Thingstad *et al*. (2014). The steady-state structure in the virus-host community is conceived to have arrived from co-evolutionary arms-race dynamics (Martiny *et al*., 2014). Briefly, new host strains evolve that have increased resistance against viral strains, while new viral strains evolve that have expanded host-range. These strain-specific arms-race dynamics are conceived to take place within multiple species. A new virus-resistant strain within a particular species experiences a cost of resistance (COR) in the form of reduced maximum growth rate. The virus associated with that species can evolve a new viral strain that re-infects the resistance-acquired strain at the cost of a reduction both in its effective adsorption coefficient to the resistance-acquired strain and in its adsorption coefficient to the previously established strains. Such co-evolutionary arms-race dynamics lead to nested infection (Flores *et al*., 2011, Jover *et al*., 2013), where some viruses (the ones present since the beginning of the arms race) are specialists, infecting the host strains that where present from early on only, whereas other viruses (the ones that evolved later on in the arms-race) are generalists, able to infect all previously evolved host strains (Fig. 1C).

The host-virus interaction model contains two mechanisms generating differences in single-cell growth rates: the reductions in maximum growth rates in strains within a species due to the acquired resistance mutations, as discussed above, and inherent differences in maximum growth potential and nutrient affinities for different species.

Given a seeding community of potential host species with particular maximum growth potential and nutrient affinities, one can calculate the number of strains and the abundance and activity for each strain that can establish at steady-state. In the chemostat (Thingstad *et al*., 2014), this is done as a function of the reservoir concentration of limiting nutrient and the dilution rate, together representing the idealized chemostat environment. In the food web setting of the combined model used here, the abundances are calculated as a function of the limiting resource (either mineral-nutrient or organic carbon) and the grazing loss. The limiting resource in its dissolved form in the food web setting corresponds to the reservoir concentration of the limiting resource in the chemostat, while the grazing loss corresponds to the dilution rate in the chemostat. Simulating the conceived evolutionary dynamics for the virus-host interaction model goes beyond the scope of this study.

We subsequently refer to the combination of these two models (Fig. 1) as the coupled model. As a first approximation to understanding microbial ecosystem structure, the analysis is a derivation of the steady state relationships of this coupled model. Steady states by definition have no time dependence and therefore contain no cause-effect chains. They do, however, express links between the state variables, which generally depend on the environmental drivers and the model parameters describing biological properties and interactions. We subsequently use the term "control" to mean that a state variable is linked to other variables, parameters or external drivers through these steady state relationships.

Deriving relationships in the M-limited case

Central equations describing the control in the coupled model are summarized in Box 1. The discussed relationships are obtained step-wise (details follow below; Supporting Information code 1):

(1) Derive outer constrains on bacterial community (i.e., total size B_T and limiting resource concentration) from the "minimum" PFT model.
(2) Calculate growth curves for bacterial strains of different species based on arms-race considerations.
(3) Identify established bacterial strains in the seeding community through criteria from (1) to obtain characteristics of established bacterial community and derive flagellate grazer abundance.
(4) Based on established bacterial community, calculate bacterial production (BP), virus abundance, partitioning of BP and finally VBR.

Step 1: Outer constrains on bacterial community. Analytical solutions for the bacterial side of the minimum food web model (PFTs connected by bold arrows in Fig. 1A) are obtained by assuming food consumption to be proportional to food concentration. In the M-limited situation, this

Box 1. Central equations of control of the coupled system at steady-state. Symbols and parameter values are summarized in Table 1. Derivations of the equations are given in the Supporting Information – Model Equations. For a description of the model see Theory and Methods.

Ciliates proportional to bacterial abundance and limiting mineral nutrient (used in step 1).

In the M-limited situation, total bacterial abundance (B_T) and concentration of limiting mineral nutrient (S_m) can both be related to ciliate abundance (C) through the two relationships (Supporting Information 1):

$$B_T(C) = \frac{\alpha_C}{Y_H \alpha_H} C \tag{1a}$$

and

$$S_m(C) = \frac{\alpha_C}{\alpha_A} C, \tag{1b}$$

where α_C is the clearance rate of ciliates for flagellates, α_H is the clearance rate of heterotrophic flagellates for bacteria, α_A is the affinity of autotrophic flagellates for the limiting mineral nutrient and Y_H is the yield of heterotrophic flagellates grazing on bacteria.

Viral resistance reduces maximum growth rates (used in step 2).

Starting with a parent strain in species x that has a maximum growth rate $\mu_0^{\max}$, there are i new strains after i successive resistance mutations in species x. The strain with index i, which is characterized by having the last (i-th) resistance mutation plus all previous resistance mutations, has a reduced maximum growth rate

$$\mu_i^{\max} = \mu_0^{\max} v^i, \tag{2}$$

where v ($0 < v \leq 1$) is the fractional decrease in $\mu^{\max}$ for each resistance mutation.

Uniform grazing gives grazing loss equal to slowest bacterial growth (used in step 3).

Assuming grazing from heterotrophic flagellates (H) to be non-selective and proportional to food concentration, all bacterial strains will have a grazing loss rate δ_B:

$$\delta_B = \alpha_H H = \mu_{\min} \tag{3}$$

where α_H is the clearance rate of H es for bacteria and $\mu_{\min}$ is the minimum growth rate balancing the grazing loss. $\mu_{\min}$ is the growth rate of the last evolved strain that grows just as fast as it is lost to grazing, and can thus not support any viruses. Strains established earlier in the arms-race are infected by at least one virus and thus experience loss to both viral lysis and grazing. In order to balance the additional loss to viral lysis at steady-state, strains established earlier in the arms-race require faster growth rates than $\mu_{\min}$ of the last established strain (see text).

Total abundance of bacterial species *x* and associated virus species *x* (used in step 4).

We use trade-offs between host range and effective adsorption in the viral population allowing for coexistence of specialist and generalist viruses in nested infection networks (Jover et al. 2013). With the resulting modifications in effective adsorption coefficients for pairs of mutated hosts and viruses (Supporting Information 5), the number of individuals in each strain and the total abundance of each bacterial species ${}_xB_T$ for a given abundance of C and H is calculated as (Supporting Information 6):

$${}_xB_T(C,H) = {}_xB_0 \left[1 + \frac{1 - {}_x\sigma\, {}_x\rho}{1 - {}_x\rho} \cdot \left({}_x\rho^{-({}_xn-1)} - 1 \right) \right], \tag{4}$$

where ${}_xB_0$ is the virus-controlled abundance of the nonmutant parent strain of species x, ${}_x\sigma$ is the memory in viruses of species x to infect earlier evolved host strains and ${}_x\rho$ is the fractional decrease in effective viral adsorption for each step in extended host range of viruses in species x.

Following Thingstad et al. (2014), the abundance of viruses belonging to each species x can be calculated from summing viral abundances over strains of species x as (Supporting Information 7):

$$ {}_xV_T = {}_xB_0^{-1}\left\{ {}_xc_0(S_m) + (1 - {}_x\sigma\, {}_x\rho\ ) \sum_{k=1}^{{}_xn-1} \frac{{}_xc_k(S_m)x}{\rho^k} \right\}, \quad (5) $$

where ${}_x\beta_0$ is the viral adsorption coefficient of the original virus on the parent strain in species x and ${}_xc_0(S_m)$ is the specific loss rate of the parent strain to viral lysis (see text).

Balance of bacterial carbon demand and supply rate of carbon (used in C-limited case). With the supply rate of carbon being less than the bacterial carbon demand under M-limitation ($\Psi < \mathrm{BCD}_m$), the pool of biodegradable organic-C in Fig. 1A is depleted and the system state changes to C-limitation. Equation 1b is then no longer valid. Instead, the steady state bacterial carbon demand under C-limitation, $\mathrm{BCD}_c(S_c)$ must balance the supply rate Ψ:

$$ \mathrm{BCD}_c(S_c) = \Psi \quad (6) $$

where S_c is the concentration of the limiting C-substrate.

gives a total bacterial abundance (B_T) and concentration of limiting mineral nutrient (S_m) both proportional to ciliate abundance (Eq. 1a and 1b; symbols and parameter values are summarized in Table 1). Ciliates thus set the carrying capacity of the bacterial community in the M-limited case.

Step 2: Growth curves of seeding community. We assume a seeding community of bacterial species with specific growth rates following Michaelis-Menten kinetics, parameterized with a species-specific maximum growth rate μ^{max} and nutrient affinity α (Table 2 summarizes seeding community). Following Thingstad *et al.* (2014), host mutations give new, additional strains within a species. The mutations are conceived from a host-virus arms race and are associated with a COR in the form of a reduction in μ^{max} by a factor v ($0 < v \leq 1$) for each resistance mutation (Fig. 1C, Eq. 2). For each species, this gives a set of growth curves for its strains (Fig. 3A). For the purpose of illustration we use a seeding community of only five host species and assume a trade-off between μ_0^{max} and α defining the species such that high μ_0^{max} gives low α and vice versa, following optimal uptake kinetics (Smith and Yamanaka, 2007; Smith *et al.*, 2009), other species properties being identical. This gives a set of growth curves for the undefended parent strains of the five seeding species as illustrated in Fig. 3B. For visual clarity, the families of curves for the mutant strains in each species (as shown in Fig. 3A for species #3) are omitted in Fig. 3B. The competitive abilities of a species is thus described by the three parameters α (nutrient affinity), μ_0^{max} (maximum growth rate of parent strain) and v (where $1 - v$ is the COR).

Step 3: Criteria for established strains and derivation of grazer abundance. The vertical line in Fig. 3A and B represents the steady state concentration S_m of the limiting nutrient, which, in the M-limited case, is proportional to ciliate abundance C (Eq. 1b). Summing up strains from fastest strains (i.e., parent strains present since the beginning of the arms-race) to slow growing strains (i.e., strains established ways into the arms-race through resistance-mutations) downward along the vertical line until total bacterial abundance (B_T), given by C, is reached, gives the minimum growth rate (μ^{min}) established in the community. This μ^{min} is represented by the horizontal line in the growth curve figures (Fig. 3A and B).

Assuming grazing from heterotrophic flagellates (H) to be nonselective (although see Supporting Information 3), all bacterial strains have an equal grazing loss rate δ_B that is proportional to H (Eq. 3) and the horizontal line (μ^{min}) in Fig. 3A and B must also equal the grazing loss rate δ_B. This follows from considering the virus-host arms-race dynamics under uniform grazing: An infection of a strain by a virus implies that some of the biomass otherwise bound in the strain's biomass gets shunted back to the dissolved limiting resource pool. This dissolved resource pool, made available by viruses, represents a niche for a mutant, virus-resistant strain to evolve in the arms-race (at a resistance cost of reduced growth rate compared to the previously established, susceptible strains). This new resistant host then represents an available resource for a new virus to evolve, which has a broader host range to infect this most recently added host strain. These steps of adding new strains can only be repeated as long as the growth rates of the resistance-acquired host strains do not underscore the minimum growth rate set by the uniform grazing loss. Hence, the last strain that can establish is the strain that grows just as fast as the grazing loss rate. At this growth rate, it can only compensate for grazing loss but not viral loss. The last established strain in the system can thus not support any viruses and remains virus free.

It follows from this that the horizontal line in Fig. 3 represents both the minimum growth rate μ^{min} established in the community and the grazing loss rate δ_B. Strains with

Table 1. Symbols and parameter values used in the model.

Parameter	Description	Value, unit
State variables		
B_T	Total bacterial abundance	ml^{-1}
${}_xB_0$	Number of individuals of undefended parental bacterial strain B_0 of species x	ml^{-1}
${}_xB_i$	Number of individuals of mutant strain i of bacterial species x	ml^{-1}
${}_xB_T$	Total abundance of bacterial species x	ml^{-1}
V_T	Total virus abundance	ml^{-1}
${}_xV_T$	Abundance of viruses infecting species x	ml^{-1}
C	Total ciliate abundance	Varied to test for sensitivity, ml^{-1}
H	Total heterotrophic flagellates abundance	ml^{-1}
S_m	Concentration of limiting mineral nutrient	nM P
S_c	Concentration of carbon source	nM C
${}_xn(H,C)^{xx}$	Number of established strains of bacterial species x for given abundance of flagellates and ciliates	d.l.
Affinities and clearance rates		
α_C	Clearance rate of ciliates for flagellates (autotrophic and heterotrophic)	0.0005 l nmol-P^{-1} h^{-1} = 5 * 10^{-6} L h^{-1} ind^{-1}
α_H	Clearance rate of heterotrophic flagellates for bacteria	0.0015 l nmol-P^{-1} h^{-1} = 2.5 * 10^{-8} l h^{-1} ind^{-1}
α_A	Affinity of autotrophic flagellates for S_m	0.04 l nmol-P^{-1} h^{-1}
${}_x\alpha_0$	Affinity of parental strain of bacterial species x for S_m or S_c	l nmol-P^{-1} h^{-1}
${}_x\alpha_i$	Affinity of mutant strain i of bacterial species x for S_m or S_c	l nmol-P^{-1} h^{-1}
BCD_m	Bacterial carbon demand in M-limited case	nM C h^{-1}
BCD_c	Bacterial carbon demand in C-limited case	nM C h^{-1}
ψ	Supply rate of carbon	Varied to test for sensitivity, nM C h^{-1}
Maximum growth rates		
${}_x\mu_0^{max}$	Maximum specific growth rate of parental bacterial strain of species x	h^{-1}
${}_x\mu_i^{max}$	Maximum specific growth rate of bacterial strain i of species x	h^{-1}
Properties of grazing interactions		
${}_xv$	Fractional decrease in μ_i^{max} for each mutation giving new strain in species x	d.l.
$COR = 1 - {}_xv$	COR of species x	d.l.
δ_B	Specific grazing loss rate of bacteria	h^{-1}
Y_{BC}	Yield from bacterial carbon consumption	0.4
Y_H	Yield from heterotrophic flagellate predation	0.3
Properties of host-virus interactions		
${}_x\rho$	Fractional decrease in effective viral adsorption coefficient β for each step in increased host range in species x	0.9 d.l.
${}_x\sigma$	"Memory" in viruses describing the ability to infect previous host strains in species x	0.9 d.l.
${}_x\beta_0$	Effective adsorption coefficient for the interaction between parental bacterial strain of species x and its virus	1.5 × 10^{-10} L h^{-1}
${}_x\beta_i$	Effective adsorption coefficient for the interaction between bacterial strain i of species x and its virus	L h^{-1}
${}_xc_i$	Specific loss rate of strain i of species x to viral lysis	h^{-1}
Conversion factors		
P per bacterial cell (PperB)		3.33 × 10^{-8} nmol P $cell^{-1}$
P per heterotrophic nanoflagellate cell (PperH)		1.67 × 10^{-5}nmol P $cell^{-1}$
P per ciliate cell (PperC)		1 × 10^{-2} nmol P $cell^{-1}$
Molar C:P ratio in bacterial biomass (CtoPperB)		50

Parameter values are adapted from Thingstad *et al.* (2007) and viral adsorption coefficient corresponds to Weitz (2015).

Table 2. Parameter values used for parental strains in seeding community consisting of five bacterial species (for parameter description, see Table 1).

Bacterial species	1	2	3	4	5
${}_xB_0$ (ml^{-1})	5.00 * 10^3	5.00 * 10^3	5.00 * 10^3	5.00 * 10^3	5.00 * 10^3
${}_x\mu_0^{max}$ (h^{-1})	1.00	0.60	0.36	0.22	0.13
${}_x\alpha_0$ (l nmol-P^{-1} h^{-1}/l h^{-1} ind^{-1})	0.01/3.33 * 10^{-10}	0.02/6.67 * 10^{-10}	0.04/1.33 * 10^{-9}	0.08/2.67 * 10^{-9}	0.16/5.33 * 10^{-9}
${}_xv$	0.9	0.9	0.9	0.9	0.9
${}_x\sigma$	0.9	0.9	0.9	0.9	0.9
${}_x\rho$	0.8	0.8	0.8	0.8	0.8

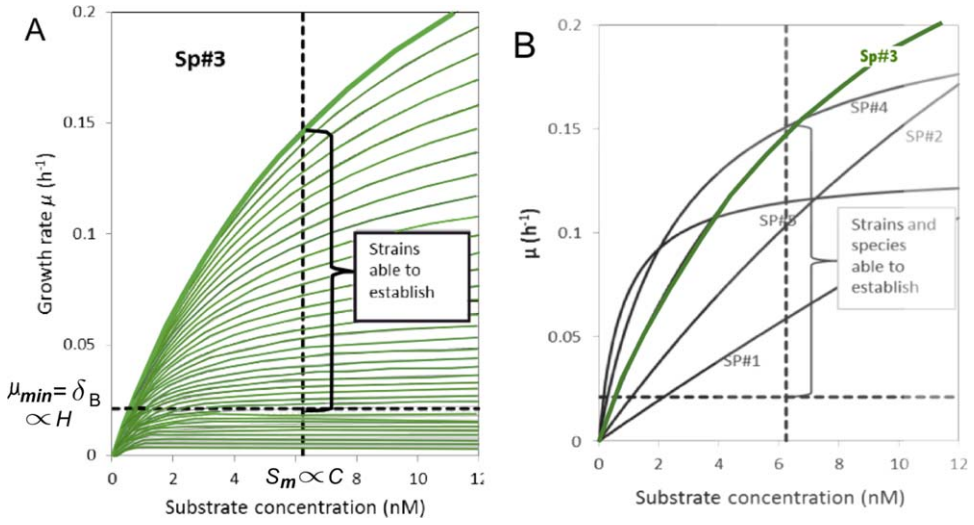

Fig. 3. Growth characteristics of the bacterial seeding community.
A: Illustration of growth rate curves for strains of Species #3 as a function of limiting substrate concentration (mineral nutrient or organic carbon). The family of growth curves reflects conceived arms-race dynamics, where the parent strain (upper most growth curve in bold green) has the highest maximum growth rate (μ_0^{max}) and evolved mutant strains have reduced μ^{max} (growth curves below parent strain shown as thin green lines, where $\mu_i^{max} = \mu_0^{max} v'$) due to COR. At steady state, only strains can establish whose growth rates at a S_m (indicated by vertical dashed line, proportional to ciliate abundance C under M-limitation) are equal to or exceed the loss rate, δ_B through grazing by H (horizontal dashed line, equivalent to minimum growth rate μ_{min} established in the BCD, see text). Growth rates of strains exceeding δ_B are compensated for by viral lysis, that is, faster growing strains experience higher loss to viral lysis than slower growing strains at steady state.
B. Growth rates of parent strains of five different seeding species as a function of S_m. For visual clarity, the families of growth curves for strains evolved from the parent strain of each species are omitted. The seeding species have a trade-off between μ^{max} (asymptote for growth rate at high substrate concentration) and nutrient affinity α (angle of growth rate at $S_m = 0$), such that a high α gives low μ^{max} and vice versa. By the same steady-state requirement as in Fig. 3A), strains of species growing equal to or faster than δ_B at a given S_m are able to establish, supporting viruses if they grow faster than δ_B (indicated with curly bracket).

growth curves passing below the crossing point between the horizontal line (minimum growth rate) and vertical line (limiting nutrient concentration) are unable to compensate for predatory loss and cannot establish. With H determining the minimum growth rate and C determining total bacterial abundance, Fig. 3 thus links the structure of the microzooplankton community to the criteria a bacterial strain has to fulfill to successfully compete in the M-limited case.

Regarding the steady state solution for H, we observe that the total bacterial abundance for a given ciliate abundance C, $B_T(C)$, is given by (Eq. 1a), but it is also the sum of abundances over all established strains of all species. Summing up abundances over established strains downwards along the vertical line in Fig. 3 until an arbitrary minimum value $\mu^{min} = \alpha_H H$ (from Eq. 3) is reached gives a community abundance $B'_T(C, H)$, determined both by C and H (curves in Fig. 4A). The steady state solution for H is found where $B_T(C)$, given by (Eq. 1a), equals $B'_T(C, H)$, given by summing up over all established strains. μ^{min} from the intersection of $B'_T(C, H)$ and $B_T(C)$ (illustrated in Fig. 4A) then gives H, using the proportionality of H with μ^{min} (Eq. 3).

To calculate the curve for $B'_T(C, H)$ in Fig. 4A, both the number of established strains and the abundance of individuals in each of these strains is needed. For M-limited growth, the number ${}_x n(C, H)$ of strains that a bacterial species x can establish at an abundance H for a given abundance C is determined by the competitive properties of the hosts, that is, their nutrient affinities, maximum growth rates and COR (Supporting Information 4, Thingstad *et al.*, 2014). To find the abundance of individuals for each strain, we follow Thingstad *et al.* (2014) and assume nested infection (Flores *et al.*, 2011; Jover *et al.*, 2013) as shown in Fig. 1C. Nested infection leads to an upper triangular host-virus interaction matrix β for each species (Supporting Information 5). The elements in β for each host-virus pair are defined by the effective adsorption coefficient β_0 of the original virus on the undefended parent strain and two attenuation coefficients ρ and σ. ρ defines the decrease in effective adsorption of infective viruses for newly established strains due to the increased resistance of the mutated strains and σ is the viral memory coefficient describing the ability of mutant viruses to infect previously established host strains (Thingstad *et al.*, 2014). ρ and σ fulfill the general trade-off conditions for coexistence in a nested infection network (Jover *et al.*, 2013; Korytowski and Smith, 2015). Knowing these modifications in effective adsorption coefficients for pairs of mutated hosts and viruses allows calculation of the number of individuals in

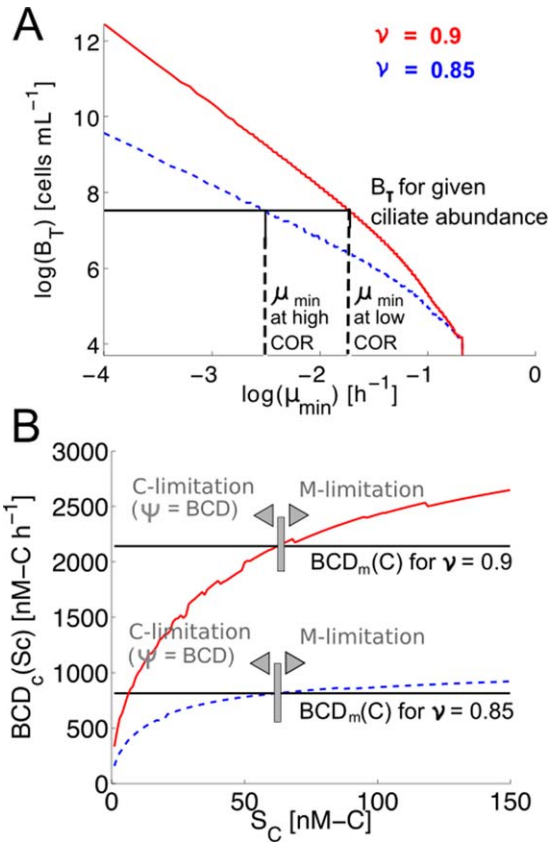

Fig. 4. Steady-state constraints determining minimum growth rate μ_{min} established in the system (A) and switch of system from C-limitation to M-limitation (B). Solid red curves for $\nu = 0.9$ (i.e., reduction of μ^{max} by 10% for acquired viral resistance, "low COR") and dashed blue curves for $\nu = 0.85$ (i.e., reduction of μ^{max} by 15%, "high COR") for ciliate abundance of 50 cells ml^{-1}. A: Total bacterial abundance B_T from summing up strains from fastest growing to slowest growing strain with arbitrary μ_{min} as function of arbitrary μ_{min}. At steady state, μ_{min} of the latest established strain must equal the loss rate δ_B from grazing by H (as discussed in Fig. 3A) and μ_{min} established in the system is thus proportional to H. The intersection of B_T for a given ciliate abundance (from Eq. 1a, black horizontal line in Fig. 4A) and the curves for B_T as a function of μ_{min} gives μ_{min} at steady-state, from which H is derived (see text). B: BCD carbon demand under C-limitation from summing up production in carbon units of established strains from fastest to slowest growing strains as a function of limiting C-substrate S_c [$BCD_c(S_c)$]. High growth rates at high S_c lead to high $BCD_c(S_c)$. Under C-limitation, all of the supplied carbon gets assimilated and the supply rate ψ equals $BCD_c(S_c)$. BCD for a given ciliate abundance under M-limitation [$BCD_m(C)$] is indicated by horizontal black lines. BCD exceeding $BCD_m(C)$ under M-limitation is not feasible as the system switches from C-limitation to M-limitation for $\psi > BCD_m(C)$.

each strain and total abundance of each bacterial species ${}_xB_T$ for a given abundance of C and H (Eq. 4). Summing up the abundance of individuals over all species x gives $B'_T(C,H)$ (curves in Fig. 4A). With H determined for a given value of C through $B_T(C) = B'_T(C,H)$ using the proportionality of H and μ^{min} (done in Fig. 4A), one can calculate H as a function of C (Fig. 5A, top).

Step 4: Properties of established bacterial and viral community. The difference between the growth rate of a virus infected strain i from bacterial species x at substrate concentration S_m (${}_x\mu_i(S_m)$) and its loss to predation (δ_B) is the specific loss rate ${}_xc_i(S_m)$ of the strain to viral lysis (${}_xc_i(S_m) = {}_x\mu_i(S_m) - \delta_B$). Multiplying this specific loss rate with strain abundance ${}_xB_i$ and summing up over established strains and species gives the loss of bacterial production to viral lysis and thus allows calculation of the partitioning of production between lysis and predation (Fig. 5C, top). Following Thingstad *et al.* (2014), the abundance of viruses belonging to each species x can be calculated from summing viral abundances over strains of species x (Eq. 5). Summation over all species gives the total viral abundance V_T (Fig. 5B, top). From this and knowing B_T as a function of C (Eq. 1a), VBR is calculated as a function of C (Fig. 6, top).

Deriving relationships in the C-limited case

The bacterial community in the M-limited case has, for a given ciliate abundance, a bacterial carbon demand $BCD_m(C)$, which corresponds to the BP in carbon units (Supporting Information code 2). The supply rate Ψ of degradable organic-C from autochthonous and/or allochthonous sources in the system has to balance or exceed this carbon demand for the M-limited state to be sustained. With $\Psi > BCD_m$, the excess supply of organic-C can theoretically accumulate (Thingstad *et al.*, 1997), while with $\Psi < BCD_m$, the pool of biodegradable organic-C in Fig. 1A is depleted and the system state changes to C-limitation. Ciliates then no longer control the limiting nutrient (Eq. 1b). Instead, the steady state bacterial carbon demand (BCD) under C-limitation, $BCD_c(S_c)$ must balance the supply rate Ψ (Eq. 6). It is then the supply rate Ψ that determines the position of the vertical line demarking the limiting substrate concentration in the analogs to Fig. 3A and B. Instead of S_m (which is proportional to the ciliate abundance), these analogs have the concentration S_c of the limiting C-substrate on the x-axis. For a given S_c, one can now calculate the total community carbon demand $BCD_c(S_c)$ [curves in Fig. 4B], corresponding to the production in carbon units of the total bacterial community as follows: Summing up production of strains from fastest to slowest growing strains as a function of S_c until total community size $B_T(C)$ is reached gives $BCD_c(S_c)$ as well as the minimum growth rate μ^{min} of the last established strain, as in the M-limited case. From this, the abundance of heterotrophic flagellates H as a function of S_c can be calculated as in the M-limited case ($\mu^{min} = \alpha_H H$ from Eq. 3). From H as a function of S_c and $BCD_c(S_c)$ as a function of S_c (Fig. 4B) and knowing that $BCD_c(S_c)$ corresponds to the supply rate Ψ of carbon under C-limitation, we can plot H as a function of Ψ (Fig. 5A, bottom). Calculating total virus abundance V_T as a

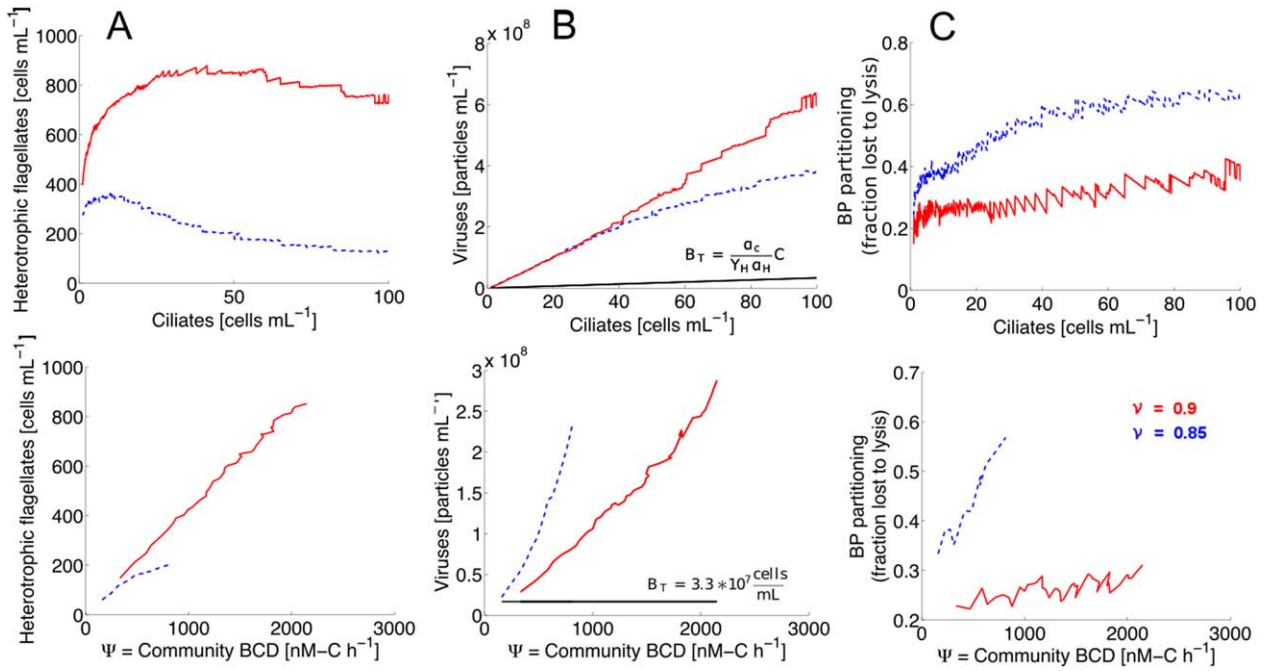

Fig. 5. Comparison of M-limited (top) and C-limited (bottom) scenario with respect to effects of COR on food web structure and function of the BCD. Abundances of heterotrophic flagellates *H* (A), viruses and total BCD (B) and partitioning of BP (C) for two different values of COR (solid red: $\nu = 0.9$, i.e., "low COR" and dashed blue: $\nu = 0.85$, i.e., "high COR"). In the M-limited case (top), ciliate abundance is chosen as an independent variable due to the central role of ciliates in controlling BCD (see text). Under C-limiation (bottom), the carbon supply rate ψ plays an analogous role to ciliates in determining the limiting substrate concentration (see text). Ciliate abundance is fixed to 50 cells ml^{-1} for C-limitation. For $\psi > \mathrm{BCD_m}(C)$, the system switches to M-limitation (Fig. 4B). Curves under C-limitation are hence only shown for values of $\psi = \mathrm{BCD_c}(S_c) < \mathrm{BCD_m}(C)$. *H* is calculated from μ_{min} that is established in the community as shown in Fig. 4A (see text). Total virus abundance is calculated from summing up viruses over all established strains of all species, where virus abundance of strain *i* is proportional to strain *i*'s growth rate and μ_{min} (Eq. 4 and Supporting Information S30).

function of S_c (Eq. 5) and using the relationship of S_c and $\mathrm{BCD_c}(S_c) = \Psi$ (Fig. 4B), we get V_T (Fig. 5B, bottom), the fraction of BP lost to viral lysis (Fig. 5D, bottom) and VBR (Fig. 6, bottom) as a function of Ψ. The maximum value of Ψ before the system switches from C-limitation to M-limitation is given by the carbon demand under M-limitation [$\mathrm{BCD_m}(C)$, horizontal lines in Fig. 4B]. Curves for C-limitation at the bottom in Figs. 5 and 6 are hence only shown for supply rates $\Psi = \mathrm{BCD_c}(S_c) < \mathrm{BCD_m}(C)$.

Results and discussion

The presented framework is a conceptual tool that shows how internal (e.g., strain- and species competition and defense against strain-specific viruses with associated COR) and external control mechanisms of the bacterial community (nonselective grazing and competition between different PFT) may regulate VBR in pelagic environments. Rather than quantitatively predicting community dynamics using fine-tuned parameters, we show how internal and external control factors may be linked in intricate ways. This should appeal microbial ecologists to increasingly consider different scales in this complex system simultaneously. At this stage, the framework represents a hypothesis that needs to be tested with data.

A theoretical framework for VBR

VBR has been measured in pelagic environments for over 25 years and although VBR is frequently referred to as 10:1, VBR is highly variable in aquatic systems, spanning over four orders of magnitude in size (Proctor and Fuhrman, 1990; Tapper and Hicks, 1998; Danovaro and Serresi, 2000; Clasen *et al.*, 2008; Wigington *et al.*, 2016). A clear understanding of mechanisms regulating this number is still lacking. Our modeling work suggests that this lack may in part be due to a segregation in microbial ecology where different scales have traditionally been studied separately. The analysis made here, where we link mechanisms controlling diversity inside the bacterial community with external control shows a possible theoretical foundation for VBR, and thus suggests a potential for improved analysis of existing data. Essentially, our framework predicts that VBR emerges as the ratio between mechanisms acting internally to the bacterial community, such as competition between strains and resistance against strain-specific viruses and trade-offs between organism traits,

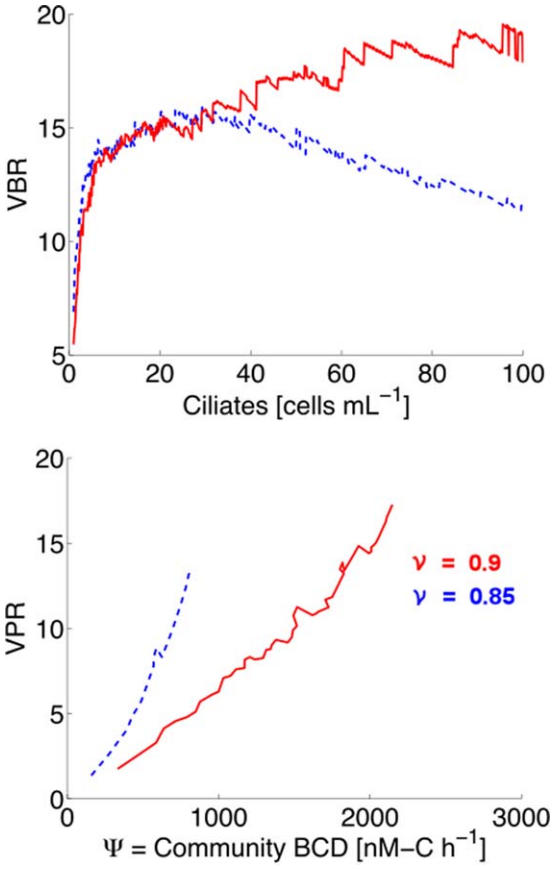

Fig. 6. VBR as a function of the independent variables (ciliates in M-limited, top and carbon supply rate ψ in C-limited case, bottom) for two different values of COR (solid red: $\nu = 0.9$, i.e., "low COR" and dashed blue: $\nu = 0.85$, i.e., "high COR"). Ciliate abundance in C-limited case is 50 cells ml^{-1}. VBR is calculated as the ratio of the total virus and BCD abundance show in in Fig. 5B.

which regulate strain- and species level diversity and mechanisms acting externally, such as competition and grazing between different PFTs (Figs. 2 and 6).

Specifically, our combined model assumes a predator control of total bacterial abundance B_T (the denominator of VBR). This is in line with expected impacts of grazing on total bacterial biomass (Gonzales *et al.*, 1990; Sherr *et al.*, 1992; Hansen *et al.*, 1997; Pasulka *et al.*, 2015), where rapid response of flagellate grazing seems consistent with the relatively stable abundance of 10^6 bacterial cells ml^{-1} in marine environments (Azam *et al.*, 1983). Although we note that grazing can be important to mediate phenotypic diversity in the BCD (Gasol *et al.*, 1999), our assumption is in line with grazers having weaker effects on genotypic BCD composition (Baltar *et al.*, 2015) than lytic viruses have (Brussaard, 2004; Weinbauer, 2004; Bouvier and del Giorgio, 2007; Lima-Mendez *et al.*, 2015). Viral lysis is the only loss mechanism included in our model to compensate for differences in host growth rates. Total viral abundance V_T (the numerator of VBR) is therefore determined by the steady state requirement that any growth of a strain exceeding the uniform grazing loss must be balanced by viral lysis. As discussed above, this implies that the last established strain growing at $\mu^{min} = \delta_B$ does not support any viruses, while virus-infected strains support more and more viruses the earlier they were established (i.e., the faster their growth rates are relative to μ^{min}). *Hence, central to this model is that total virus abundance increases for increasing host growth rate spectra*.

Despite being conceptually relatively simple, these assumptions link diversity and function in a somewhat intricate and circular manner: It is viruses that allow host groups with different growth rates to co-exist, while it is the magnitude of these differences between growth rates that determine how many viruses are needed for coexistence (Thingstad, 2000). Since COR generates such differences in growth rate, this links COR to viral abundance (Fig. 5B) and thus VBR (Fig. 6).

To scrutinize the presented theory, the prediction that V_T is tightly coupled to the width of the host community growth rate spectrum needs to be tested. Using the incorporation of a fluorescent amino-acid analog, Samo *et al.* (2014) recently reported host growth rate spectra to follow a power-law distribution with slow growing hosts dominating, but with slopes of the distribution varying between samples. With low slopes allowing for larger host growth rate differences in the sample, this suggests that correlating VBR values in a given environment with the slope of such spectra may be a way to experimentally challenge the theoretical framework.

Strong sensitivity of diversity, food web structure and ecosystem function to COR

A conspicuous result in our analysis is that species diversity and food web structure on the level of PFT, as well as biodiversity-ecosystem function (Figs. 4–7), are highly sensitive to the trade-off between competitive and viral defense abilities (COR) inside the bacterial community. Although COR can be difficult to measure and may depend on the environments (Bohannan *et al.*, 2002), it has been experimentally verified in chemostats and natural communities (Lenski and Levin, 1985; Bohannan *et al.*, 2002; Middelboe *et al.*, 2009; Avrani *et al.*, 2011). Regardless, rather than suggesting a particular magnitude of COR for a specific microbial system, our model illustrates how sensitive a microbial community appears to be in terms of its structure and function given any particular value of COR.

In this analysis, we assume two slightly different values of COR, where high COR (i.e., $\nu = 0.85$ corresponding to a 15% reduction of μ^{max} for acquired resistance mutations) implies larger reductions in μ^{max} (COR $= 1 - \nu$). This larger reduction in μ^{max} compared with lower COR increases the spacing between the growth rate curves in Fig. 3A, leading

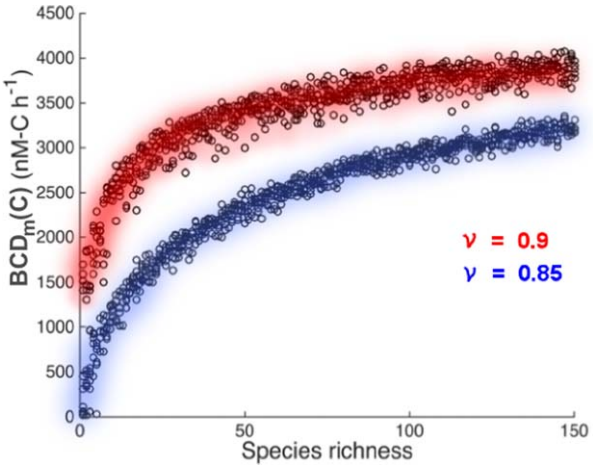

Fig. 7. In-silico experiment demonstrating the effect of species richness on BCD carbon demand under M-limitation [$BCD_m(C)$] for low (red, $\nu = 0.9$) and high (blue, $\nu = 0.85$) COR. Each point represents one composition of the seeding community. For each species richness, five repeated experiments were done drawing maximum growth rates μ^{max} for each species from a uniform distribution between 0 and 1.0 h^{-1} and assuming the same range and trade-off for nutrient affinity α as in seeding community of Fig. 3B (i.e., high α implies low μ^{max} and vice versa). Ciliate abundance is 50 ciliates ml^{-1}, other parameters as in Table 1.

to a lower position of the horizontal line and thus a lower minimum growth rate μ_{min} established in the system (illustrated graphically in Fig. 4A). Due to the smaller μ_{min} and a subsequently higher proportion of slow growing strains established in the bacterial community, whose total size is given independently of COR by ciliates (Eq. 1a), total BP is reduced for high COR. As a consequence, total bacterial carbon demand is lower for high COR relative to low COR (Fig. 4B). Hence, both viral and grazer community abundances are reduced for high COR under M-limitation [comparing blue curves in Fig. 5A and B (top) relative to red curves], which is also reflected in the lower VBR for high COR (Fig. 6, top). In addition, since high COR leads to a reduction of μ_{min} and since heterotrophic flagellates H are proportional to μ_{min} through (Eq. 2), the abundance of H is reduced for high COR. As a consequence, the partitioning of BP is in favor of the viral community and more of the BP is lost to lysis. *Critical for biogeochemical functioning, food web transfer efficiency is hence reduced for high COR (Fig. 5C, top).*

Analogous to ciliates determining the limiting mineral nutrient concentration S_m in the M-limited case (Eq. 1b), the carbon supply rate (ψ) determines the BCD and hence sets the growth constraint under C-limiation [$BCD_c(S_c)$]. The limiting carbon concentration S_c is found from $BCD_c(S_c)$ as discussed for Fig. 4B. Analogous to ciliates under M-limitation, ψ is therefore chosen as an independent variable for C-limitation (Fig. 5, bottom). Under C-limitation, the highest maximum abundances of H and viruses can be reached at low COR (red curves go beyond blue curves in Fig. 5A and B, bottom), since low COR can supply higher supply rates ψ before the system switches from C- to M-limitation (horizontal line for low COR is higher in Fig. 4B than for high COR). However, for any given supply rate ψ corresponding to $BCD_c(S_c)$, a high COR (blue curve in Fig. 5B, bottom) gives higher virus abundances than low COR (red curve in Fig. 5B, bottom). This is explicable by the viruses' role as compensators for growth rate differences in the host strains when assuming nonselective grazing (Eq. 5 and Supporting Information 7).

Since high COR reduces μ_{min}, growth rate differences between the fastest and slowest growing strains in the BCD increase and hence more viruses are supported for high COR (Fig. 5B, bottom). This is opposite to the abundance of H, which is lower at high COR for any given ψ corresponding to $BCD_c(S_c)$ (Fig. 5A, bottom) due to the reduction of μ_{min} at high COR (Fig. 4A) and the proportionality of H with μ_{min} (Eq. 3). *As in the M-limited case, high COR thus implies reduced transfer efficiency and a larger fraction of BP begin lost to lysis (blue curve in Fig. 5C, bottom). Understanding biogeochemical functioning of the pelagic microbial community is thus in our framework predicted to strongly rely on an increased understanding of trade-offs between organism traits.*

Strong sensitivity of biodiversity, food web structure and ecosystem function on seeding community

We only included one trade-off between the nutrient affinity parameters α and maximum uptake rates μ^{max} describing the seeding community (Table 2). This trade-off has been explained physiologically in optimal uptake kinetics (Smith *et al.*, 2009) and seems supported by data compilations (Litchman *et al.*, 2007), although Fiksen *et al.* (2013) discuss how this trade-off may not be valid under diffusion limitation. Regardless, the set of trade-offs linking parameters in the seeding community must in reality be complex. One can, for example, speculate that CRISPR defense systems are expensive to run (lowering a species' μ^{max}), but adding a new recognition sequence is cheap (Kang *et al.*, 2013), such that the reduction in μ^{max} from one resistance mutation to the next may be small (such that ν would be close to 1 in our model), creating a trade-off between COR and μ^{max}. Again, our future level of understanding of the system depends on unraveling these trade-offs (Litchman *et al.*, 2015).

Our choice of seeding community and trade-off is crucial for how community composition varies, as is evident from inspecting Fig. 3B: High S_m (or S_c) tend to favor species with high μ^{max}, while low S_m or S_c favor species with high α_m or α_c in the M- and C-limited cases, respectively. This has interesting consequences for species diversity in terms

of ciliate abundance (Supporting Information – Ciliate Effects).

In addition, affinity for mineral nutrient S_m (α_m) and affinity for carbon S_c (α_c) are proportional in our seeding community. The consequence is that a shift between the C- and M-limited states is not expected to affect BCD. An alternative assumption could be that there is a trade-off between being a C-specialist and an M-specialist. This would give a re-shuffling of the growth curves in Fig. 3B as the type of limitation changes, accompanied by shifts in BCD. *Vibrio splendidus* growing into large, carbon storing cells dominating the bacterial community after excess glucose addition in a mesocosm system (Thingstad *et al.*, in press) are an interesting example where α_m varied as a function of the available carbon concentration.

Emerging biodiversity-ecosystem functioning relationships fits generic theory

Biodiversity-ecosystem functioning (BEF) is a pressing issue in ecological research in general and a field where microbial research has been suggested to have a special potential to contribute (Krause *et al.*, 2014). With the mechanistic descriptions used in both the PFT and host-virus component of the coupled model, the form of these relationships can be traced back to organism properties and interactions in a more direct manner than in generalized BEF models (Connolly *et al.*, 2013), although at the expense of narrowing the relevance to the planktonic ecosystem.

Experimentally, an effect of species richness on ecosystem function has been shown by combining bacterial isolates and measuring respiration rates as the ecosystem response (Bell *et al.*, 2005). Our coupled model allows *in-silico* experiments of this kind as demonstrated by an exploration of the effect of species richness on bacterial carbon consumption, $BCD_m(C)$ (Fig. 7). Within the range investigated here, the effect of the COR parameter v on $BCD_m(C)$ persists also at high richness. The shape of the curve in Fig. 7 derived from our mechanistic model resembles the generalized response to richness derived by Connolly *et al.* (Fig. 6 in Connolly *et al.*, 2013) for values of their Θ-parameter between 0.5 and 1, where Θ describes interaction strength between species. The saturation in Fig. 7 illustrates some redundancy of species effects on the ecosystem function (Bell *et al.*, 2005).

Finally, we note that steady-state implies that the assumed host-virus arms-races have developed to maturation (Thingstad *et al.*, 2014). This linking of evolutionary to ecological time scales may be relevant to our assumption of all species being substrate generalists, as it has been shown experimentally (Gravel *et al.*, 2011) that adapting species to generalist versus specialist strategies prior to combining them affected BEF-relationships.

Experimental support for the theoretical framework

Despite its simplicity, the PFT model used in this study (Fig. 1A) is able to quantitatively reproduce successions of dominant PFTs in stimulated bloom dynamics in mesocosm experiments; both in differently perturbed mesocosms started from the same initial water mass (Thingstad *et al.*, 2007) and in similarly treated mesocosms started from different initial water masses (Larsen *et al.*, 2015).

Finding strong experimental support (or refutation) for the "Killing-the-winner" models resolving the internal bacterial community structure has proven more difficult (Winter *et al.*, 2010) despite them being frequently cited in experimental work. Thingstad *et al.* (2014) recently suggested that one of the reasons for this may be in the way models and data are compared: The "Killing-the-Winner" models operate with "host-groups," the sizes of which are top-down controlled by lytic viruses. Data on bacterial diversity are typically in the form of 16S rDNA sequences and therefore refer to "species"-level (rather than "strain"-level) diversity. Theory-data comparisons therefore usually imply an assumption of the model's host-groups to correspond to a "species"-level in the data. When assuming more realistically that the model's host groups to correspond to strains, however, the number of individuals belonging to a species becomes the number of individuals per strain, summed over the strains that this species manages to establish in competition with other species in the given environment (Thingstad *et al.*, 2014). In this case, individuals per species and diversity are both top-down controlled by viruses, which affects the richness component (number of different strains) and bottom-up controlled through competition, which affects the evenness component (abundance of each strain). A logic consequence from this is that by indirectly controlling the amount of available resources through trophic cascades (Eq. 1a), grazers should have a direct effect on internal bacterial community diversity, even when assuming nonselective grazing. This strain-based host-virus model (Fig. 1B and C) fits with different aspects of microbial ecology, such as coexistence of less competitive and better defended strains with more competitive strains (Suttle and Chan, 1993; Waterbury and Valois, 1993; Holmfeldt *et al.*, 2007) and a dominance of slow growing types (Malmstrom *et al.*, 2004; Campbell *et al.*, 2011; Samo *et al.*, 2014), as well as postulated inverse rank-abundance distributions of hosts and their associated viruses (Suttle, 2007; Våge *et al.*, 2013a; Thingstad *et al.*, 2014). Specifically, it suggests that the widespread slow growth in natural populations (e.g., Samo *et al.*, 2014) is due to a dominance of defensive strains that have reduced growth rates due to COR (Thingstad *et al.*, in press). Host abundance on the species level emerges in the model from a combination of competitive and defensive abilities

(Våge *et al.*, 2013b), unifying the two previously opposing lines of argument that the success of SAR11 is based on either its defensive or on its competitive superiority (Zhao *et al.*, 2013). The "King of the Mountain" (Giovannoni *et al.*, 2013) hypothesis alternatively explains success of SAR11 based on horizontal transfer of resistance genes, allowing highly competitive strains to simultaneously be strong in defense as well. In contrast to our model, the "King of the Mountain" hypothesis does not explicitly account for the wide range in activity spectra of strains observed in SAR11 (Malmstrom *et al.*, 2004). More data on relative abundance and activity of bacterial strains and their associated viruses are required to evaluate the alternative hypotheses.

Interestingly, VBR stabilizes or decreases in our model as a function of increasing ciliate (and hence total bacterial) abundance (Fig. 6, top), which is consistent with a compilation of data from marine surveys that revealed a typical decrease of virus to microbe ratios with microbial cell density (Wigington *et al.*, 2016). For a discussion on this ciliate effect, see Supporting Information – Ciliate Effects.

Extending the scope of previous studies

Several experimental and theoretical studies have stressed the importance of the systems productivity on the extent of which top-down (grazing by heterotrophic nanoflagellates and viral lysis) and bottom-up control (mineral nutrient and organic carbon limitations) determine bacterial growth, abundance and community structure (Billen *et al.*, 1990; Gasol, 1994; Pace and Cole, 1994; Pernthaler, 2005). In a recent analysis of the role of viruses in the pelagic food web, Weitz *et al.* (2015) used a model with a "one virus – one community" structure representing the opposite extreme to the resolution used here, where virus specificity is at strain level. While this black-box approach in the Weitz *et al.* model allows for a thorough analysis of food web level effects, it does not address diversity within the host communities.

However, interesting results regarding diversity and infection network constraints within the BCD have recently been derived in a theoretical study, where coevolution of virus-host community was considered (Haerter *et al.*, 2014). Furthermore, Jover *et al.* (2013) and Korytowski and Smith (2015) derived general and chemostat-specific conditions for coexistence under nested infection, respectively. However, similar to the black-box approach, focusing on the internal resolution of the host community alone (Jover *et al.*, 2013; Haerter *et al.*, 2014; Thingstad *et al.*, 2014; Korytowski and Smith, 2015) does not allow to link organism properties and internal community structure to external food web structure and ecosystem functioning, which was a major goal of this study.

The model is strongly simplified, both in terms of resolution of the different groups, nutritional modes and virus representations. Virus-host interactions are complex and even when considering virus-host interactions in a single (bacterial) community only, intricate effects became apparent on the food web level. We argue that understanding mechanisms in a constrained setting first is a fruitful way towards complete understanding of a system with fully expressed dynamics and interactions. Since bacteria and their associated viruses numerically dominate pelagic microorganisms (Suttle, 2007), the present model focuses on an important part of the whole. Extending the model to include viruses for the nonbacterial communities will add a level of complexity that needs to be treated in a follow-up study. We note that while our model resolves varying host ranges, with presumed trade-offs in virulence and two levels of virus-host specificity (bacterial strains vs. species), resolving some of the important characteristics of complex virus-host interactions, other factors such as variation in virus life style (lysogenic vs. lytic) and decay rates surely influence VBR too. This calls for future model refinements also within the bacterial community.

Summary

- Internal and external bacterial community control factors are intricately linked.
  - ⇒ Advancing microbial ecology crucially depends on simultaneously study multiple levels of resolutions.
- Species level diversity, food web structure on the level of PFT and ecosystem function strongly depend on COR and choice of seeding community, which are based on molecular properties of virus-host interactions and growth processes.
  - ○ For example, food web transfer efficiency is reduced for high COR
  - ⇒ Quantifying trade-offs in microbial strategies is fundamental to understand microbial ecology.
- VBR depends on a combination of internal and external community control mechanisms.
  - ○ Total virus abundance is predicted to be positively correlated with the width in host growth rate spectrum, while total bacterial abundance is controlled by the external food web structure.
  - ⇒ Data linking host growth rate spectra to total virus abundance are needed to test this theory.

Conclusions

By integrating the nested virus-host infection model in a microbial food web model that resolves different PFTs, our framework considers biological mechanisms for general

conditions for coexistence (Jover *et al*., 2013). Without aiming to develop a model with fine-tuned parameters, the result is a mechanistic theory for VBR in the pelagic ecosystem (Figs. 2 and 6). It suggests how molecular properties of virus-host interactions, which are manifested, for example, in COR, may be intricately linked to the structure of the grazer community (Fig. 5A), the virus abundance and partitioning of BP (Figs. 5B and C), VBR (Fig. 6) and bacterial diversity (Fig. 7). The grazer community, in turn, sets in this framework the carrying capacity of the bacterial community (the denominator of VBR) through the central role that ciliates play in bacterial community control (Larsen *et al* 2014), both through top-down effects (grazer food chain) and bottom-up effects (control of autotrophic competitors for limiting mineral nutrient). In other words, ciliates calibrate the bacterial and virus abundances to ecologically realistic values. In a world where viruses and bacteria would be the only entities regulating each others community size through direct virus-host interactions, the relative abundance of hosts and viruses may remain unchanged, but they would end up monopolizing all resources and reach ecologically unrealistic carrying capacities.

Central to the relationships derived here is the set of species-level properties defined in the seeding community (Table 2). This five-member seeding community was chosen primarily for illustrative purposes. One could imagine expanding the proposed framework by introducing (approximations to) real species in such a list. An intellectually intriguing, but not necessarily easier alternative would be to focus on trade-offs between multiple traits and generate seeding communities with Monte-Carlo techniques (Follows *et al*., 2007) as illustrated by our *in-silico* experiment (Fig. 7). Large differences found in our analysis with respect to community structure and efficiency by which BP is transferred through the food web based on small differences in COR illustrate how our future level of understanding of this system will depend on our ability to unravel such trade-offs.

Acknowledgements

This work was financed by the European Union FP7 through the European Research Council Advanced Grant 250254 Microbial Network Organization and by the Department of Biology, University of Bergen.

Conflict of Interest

The authors declare no conflict of interest.

References

Avrani, S., Wurtzel, O., Sharon, I., Sorek, R., and Lindell, D. (2011) Genomic island variability facilitates Prochlorococcus-virus coexistence. *Nature* **474:** 604–608.

Azam, F., Fenchel, T., Field, J.G., Gray, J.S., Meyerreil, L.A., and Thingstad, F. (1983) The ecological role of water-column microbes in the sea. *Mar Ecol Prog Ser* **10:** 257–263.

Baltar, F., Palovaara, J., Unrein, F., Catala, P., Hornak, K., Simek, K., et al. (2015) Marine bacterial community structure resilience to changes in protis predation under phytoplankton bloom conditions. *ISME J* **10:** 568–581.

Bell, T., Newman, J.A., Silverman, B.W., Turner, S.L., and Lilley, A.K. (2005) The contribution of species richness and composition to bacterial services. *Nat Rev Microbiol* **436:** 1157–1160.

Billen, G., Servais, P., and Becquevort, S. (1990) Dynamics of bacterioplankton in oligotrophic and eutrophic aquatic environments - Bottom-up or top-down control. *Hydrobiologia* **207:** 37–42.

Bohannan, B.J.M., Kerr, B., Jessup, C.M., Hughes, J.B., and Sandvik, G. (2002) Trade-offs and coexistence in microbial microcosms. *Anntonie van Leeuwenhoek* **81:** 107–115.

Bouvier, T., and del Giorgio, P.A. (2007) Key role of selective viral-induced mortality in determining marine bacterial community composition. *EMI* **9:** 287–297.

Brussaard, C.P.D. (2004) Viral control of phytoplankton populations - a review. *J Eukaryot Microbiol* **51:** 125–138.

Campbell, B.J., Yu, L., Heidelberg, J.F., and Kirchman, D.L. (2011) Activity of abundant and rare bacteria in a coastal ocean. *PNAS* **108:** 12776–12781.

Clasen, J.L., Brigden, J.S., Payet, J.P., and Suttle, C.A. (2008) Evidence that viral abundance across oceans and lakes is driven by different biological factors. *Freshwater Biol* **53:** 1090–1100.

Connolly, J., Bell, T., Bolger, T., Brophy, C., Carnus, T., Finn, J.A., and al, e. (2013) An improved model to present the effects of changing biodiversity levels on ecosystem function. *J Ecol* **101:** 344–355.

Danovaro, R., and Serresi, M. (2000) Viral density and virus-to-bacterium ratio in deep-sea sediments of the Eastern Mediterranean. *Appl Environ Microbiol* **66:** 1857–1861.

Fiksen, Ø., Follows, M.J., and Aksnes, D.L. (2013) Trait-based models of nutrient uptake in microbes extend the Michaelis-Menten framework. *Limnol Oceanogr* **58:** 193–202.

Flores, C.O., Meyer, J.R., Valverde, S., Farr, L., and Weitz, J.S. (2011) Statistical structure of host–phage interactions. *PNAS USA* **108:** E288–E297.

Follows, M.J., Dutkiewicz, S., Grant, S., and Chisholm, S.W. (2007) Emergent biogeography of microbial communities in a model ocean. *Science* **315:** 1843–1846.

Fuhrman, J.A. (1999) Marine viruses and their biogeochemical and ecological effects. *Nature* **399:** 541–548.

Gasol, J.M. (1994) A framework for the assessment of top-down vs. bottom-up control of the heterotrophic nanoflagellate abundance. *Mar Ecol Program Ser* **113:** 291–300.

Gasol, J.M., Zweifel, U.L., Peters, F., Fuhrman, J.A., and Hagstrom, A. (1999) Significance of size and nucleic acid content heterogeneity as measured by flow cytometry in natural planktonic bacteria. *Appl Environ Microbiol* **65:** 4475–4483.

Giovannoni, S.J., Britschgi, T.B., Moyer, C.L., and Field, K.G. (1990) Genetic diversity in Sargasso Sea bacterioplankton. *Nature* **345:** 60–63.

Giovannoni, S., Temperton, B., and Zhao, Y. (2013) Giovannoni et al. reply. *Nature* **499**. doi:10.1038/nature12388.

Gonzales, G.M., Sherr, E.B., and Sherr, B.F. (1990) Size-selective grazing on bacteria by natural assemblages of estuarine flagellates and ciliates. *Appl Environ Microbiol* **53:** 583–589.

Gravel, D., Bell, T., Barbera, C., Bouvier, T., Pommier, T., Venail, P., and Mouquet, N. (2011) Experimental niche evolution alters the strength of the diversity-productivity relationship. *Nature* **469:** 89-U1601.

Haerter, J.O., Mitarai, N., and Sneppen, K. (2014) Phage and bacteria support mutual diversity in a narrowing staircase of coexistence. *ISME J* **8:** 2317–2326.

Hansen, P.J., Bjørnsen, P.K., and Hansen, B.W. (1997) Zooplankton grazing and growth: scaling within the 2-2000μm body size. *Limnol Oceanogr* **42:** 682–704.

Holmfeldt, K., Middelboe, M., Nybroe, O., and Riemann, L. (2007) Large variability in host strain susceptibility and phage host range govern interactions between lytic marine phages and their Flavobacterium hosts. *Appl Environ Microbiol* **73:** 6730–6739.

Jover, L.F., Cortez, M.H., and Weitz, J.S. (2013) Mechanisms of multi-strain coexistence in host-phage systems with nested infection networks. *J Theor Biol* **332:** 65–77.

Kang, I., Oh, H.-M., Kang, D., and Cho, J.-C. (2013) Genome of a SAR116 bacteriophage shows the prevalence of this phage type in the oceans. *PNAS USA* **110:** 12343–12348.

Korytowski, D.A., and Smith, H.L. (2015) How nested and monogamous infection networks in host-phage communities come to be. *Theor Ecol* **8:** 111–120.

Krause, S., LeRoux, X., Niklaus, P.A., Bodegom, M.V., Lennon, J.T., Bertilsson, S., and al, e. (2014) Trait-based approaches for understanding biodiversity and ecosystem functioning. *Front Microbiol* **5:** 251.

Larsen, A., Egge, J.K., Neistgaard, J.C., Di Capua, I., Thyrhaug, R., Bratbak, G., and Thingstad, T.F. (2015) Contrasting response to nutrient manipulation in Arctic mesocosms are reproduced by a minimum microbial food web model. *Limnol Oceanogr* **60:** 360–374.

Lenski, R.E., and Levin, B.R. (1985) Constraints on the coevolution of bacteria and virulent phage: a model, some experiments and predictions for natural communities. *Am Nat* **125:** 585–602.

Lima-Mendez, G., Faust, K., Henry, N., Decelle, J., Colin, S., Carcillo, F., et al. (2015) Determinants of community structure in the global plankton interactome. *Science* **348:** 1262073 1262071−1262079.

Litchman, E., Edwards, K.F., and Klausmeier, C.A. (2015) Microbial resource utilization traits and trade-offs: Implications for community structure, functioning, and biogeochemical impacts at present and in the future. *Front Microbiol* **6:** 254.

Litchman, E., Klausmeier, C.A., Schofield, O.M., and Falkowski, P.G. (2007) The role of functional traits and trade-offs in structuring phytoplankton communities: Scaling from cellular to ecosystem level. *Ecol Lett* **10:** 1170–1181.

Malmstrom, R.R., Kiene, R.P., Cottrell, M.T., and Kirchman, D.L. (2004) Contribution of SAR11 bacteria to dissolved dimethylsulfoniopropionate and amino acid uptake in the North Atlantic. *Appl Environ Microbiol* **70:** 4129–4135.

Martiny, J.B.H., Riemann, L., Marston, M.F., and Middelboe, M. (2014) Antagonistic Coevolution of Marine Planktonic Viruses and Their Hosts. *Annu Rev Marine Sci* **6:** 393–414.

Middelboe, M., Holmfeldt, K., Riemann, L., Nybroe, O., and Haaber, J. (2009) Bacteriophages drive strain diversification in a marine Flavobacterium: Implications for phage resistance and physiological properties. *Environ Microbiol* **11:** 1971–1982.

Mou, X., Sun, S., Edwards, R.A., Hodson, R.E., and Moran, M.A. (2008) Bacterial carbon processing by generalist species in the coastal ocean. *Nature* **451:** 708-U704.

Ogunseitan, O.A., Sayler, G.S., and Miller, R.V. (1990) Dynamic interactions of Pseudomonas aeruginosa and bacteriophages in lake water. *Microb Ecol* **19:** 171–185.

Øvreås, L., Forney, L., Daae, F.L., and Torsvik, V. (1997) Distribution of bacterioplankton in meromictic Lake Sælenvannet, as determined by denaturing gradient gel electrophoresis of PCR-amplified gene fragments coding for 16S rRNA. *Appl Environ Microbiol* **63:** 3367–3373.

Pace, M.L., and Cole, J.J. (1994) Comparative and experimental approaches to top-down and bottom-up regulation of bacteria. *Microb Ecol* **28:** 181–193.

Pasulka, A.L., Samo, T.J., and Landry, M.R. (2015) Grazer and viral impacts on microbial growth and mortality in the southern California Current Ecosystem. J *Plankt Res* **37:** 1–17.

Pernthaler, J. (2005) Predation on prokaryotes in the water column and its ecological implications. *Nat Rev Microbiol* **3:** 537–546.

Proctor, L.M., and Fuhrman, J.A. (1990) Viral mortality of marine bacteria and cyanobacteria. *Nature* **343:** 60–62.

Samo, T.J., Smriga, S., Malfatti, F., Sherwood, B.P., and Azam, F. (2014) Broad distribution and high proportion of protein synthesis active marine bacteria revealed by click chemistry at the single cell level. *Front Mar Sci* **1:** 1–18.

Sherr, B.F., Sherr, E.B., and McDaniel, J. (1992) Effect of protistan grazing on the frequency of dividing cells in bacterioplankton assemblages. *Appl Environ Microbiol* **58:** 2381–2385.

Smith, S.L., and Yamanaka, Y. (2007) Optimization-based model of multinutrient uptake kinetics. *Limnol Oceanogr* **52:** 1545–1558.

Smith, S.L., Yamanaka, Y., Pahlow, M., and Oschlies, A. (2009) Optimal uptake kinetics: physiological acclimation explains the pattern of nitrate uptake by phytoplankton in the ocean. *Mar Ecol Prog Ser* **384:** 1–12.

Suttle, C.A. (2007) Marine viruses - major players in the global ecosystem. *Nature Rev Microbiol* **5:** 801–812.

Suttle, C.A., and Chan, A.M. (1993) Marine cyanophages infecting oceanic and coastal strains of Synechococcus: abundance, morphology, cross-reactivity and growth characteristics. *Mar Ecol Prog Ser* **92.**

Tapper, M.A., and Hicks, R.E. (1998) Temperate viruses and lysogeny in Lake Superior bacterioplankton. *Limnol Oceanogr* **43:** 95–103.

Thingstad, T.F. (2000) Elements of a theory for the mechanisms controlling abundance, diversity, and biogeochemical role of lytic bacterial viruses in aquatic systems. *Limnol Oceanogr* **45:** 1320–1328.

Thingstad, T.F., Hagstrøm, A., and Rassoulzadegan, F. (1997) Accumulation of degradable DOC in surface waters: Is it caused by a malfunctioning microbial loop? *Limnol Oceanogr* **42:** 398–404.

Thingstad, T.F., Pree, B., Giske, J., and Våge, S. (2015) What difference does it make if viruses are strain-, rather than species-specific? *Front Microbiol* **6:**320.

Thingstad, T.F., Øvreås, L., Egge, J.K., Løvdal, T., and Heldal, M. (2005) Use of non-limiting substrates to increase size; a generic strategy to simultaneously optimize uptake and minimize predation in pelagic osmotrophs? *Ecol Lett* **8:** 675–682.

Thingstad, T.F., Våge, S., Storesund, J.E., Sandaa, R.-A., and Giske, J. (2014) A theoretical analysis of how strain-specific viruses can control microbial species diversity. *PNAS USA* **111:** 7813–7818.

Thingstad, T.F., Havskum, H., Zweifel, U.L., Berdalet, E., Sala, M.M., Peters, F., et al. (2007) Ability of a "minimum" microbial food web model to reproduce response patterns observed in mesocosms manipulated with N and P, glucose, and Si. *J Mar Syst* **64:** 15–34.

Våge, S., Storesund, J.E., and Thingstad, T.F. (2013a) Adding a cost of resistance description extends the ability of virus-host model to explain observed patterns in structure and function of pelagic microbial communities. *Environ Microbiol* **15:** 1842–1852.

Våge, S., Storesund, J.E., and Thingstad, T.F. (2013b) SAR11 viruses and defensive host strains. *Nature* **499:** E3–E4.

Waterbury, J.B., and Valois, F.W. (1993) Resistance to co-occurring phages enables marine synechococcus communities to coexist with cyanophages abundant in seawater. *Appl Environ Microbiol* **59:** 3393–3399.

Weinbauer, M.G. (2004) Ecology of prokaryotic viruses. *Fems Microbiol Rev* **28:** 127–181.

Weitz, J.S. (2015) *Quantitative Viral Ecology: Dynamics of Viruses and Their Microbial Hosts*. Princeton, NJ: Princeton University Press.

Weitz, J.S., Stock, C.A., Wilhelm, S.W., Bourouiba, L., Coleman, M.L., Buchan, A., et al. (2015) A multitrophic model to quantify the effects of marine viruses on microbial food webs and ecosystem processes. *ISME J* **9:** 1352–1364.

Wigington, C.H., Sonderegger, D., Brussaard, C.P.D., Buchan, A., Finke, J.F., Fuhrman, J.A., et al. (2016) Re-examination of the relationship between marine virus and microbial cell abundance. *Nature Microbiol.* article 15024.

Wilhelm, S.W., and Suttle, C.A. (1999) Viruses and nutrient cycles in the sea: Viruses play critical roles in the structure and function of aquatic food webs. *Bioscience* **49:** 781–788.

Winter, C., Bouvier, T., Weinbauer, M.G., and Thingstad, T.F. (2010) Trade-offs between competition and defense specialists among unicellular planktonic organisms: the "Killing the Winner" hypothesis revisited. *Microbiol Mol Biol Rev* **74:** 42–57.

Wommack, K.E., and Colwell, R.R. (2000) Virioplankton: viruses in aquatic ecosystems. *Microb Mol Biol Rev* **64:** 69–114.

Zhao, Y.L., Temperton, B., Thrash, J.C., Schwalbach, M.S., Vergin, K.L., Landry, Z.C., et al. (2013) Abundant SAR11 viruses in the ocean. *Nature* **494:** 357–360.

Supporting information

Additional Supporting Information may be found in the online version of this article at the publisher's web-site:

Fig. S1. Bacterial species composition of 5 seeding species (Fig 3B, Table 2) in different shades of gray, and Shannon index (black curve with small dots) as a function of *C* in the M-limited case. Species abundance is calculated as the sum of abundances over all established strains (SI 6). The trade-off between μmax and α in the seeding species gives a dominance of species with strong α at low *Sm* (i.e. low *C*, Eq. 1b) and a dominance of species with high μmax at high Sm (i.e. high *C*). Intermediate *C* (around 20 mL-1) gives highest Shannon diversity.